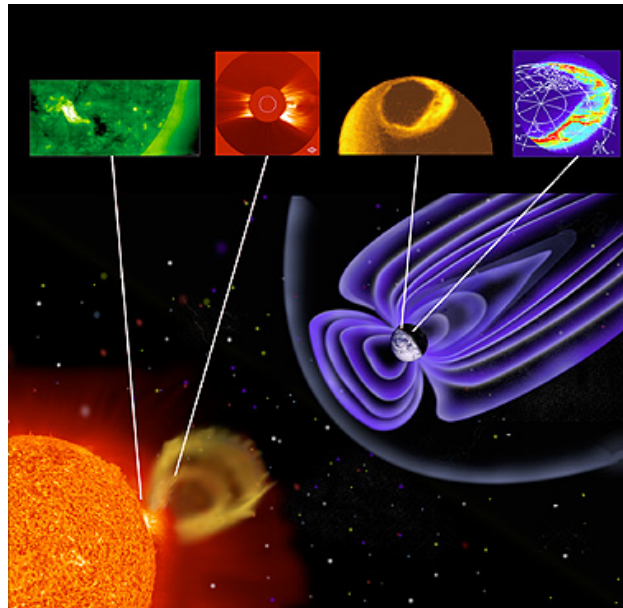


Multiscale simulation of waves in plasmas

E. Alec Johnson

Department of Mathematics, UW-Madison

Presented on June 10 at Hyp2008



©2003, Kenneth Lang, Tufts University



Outline

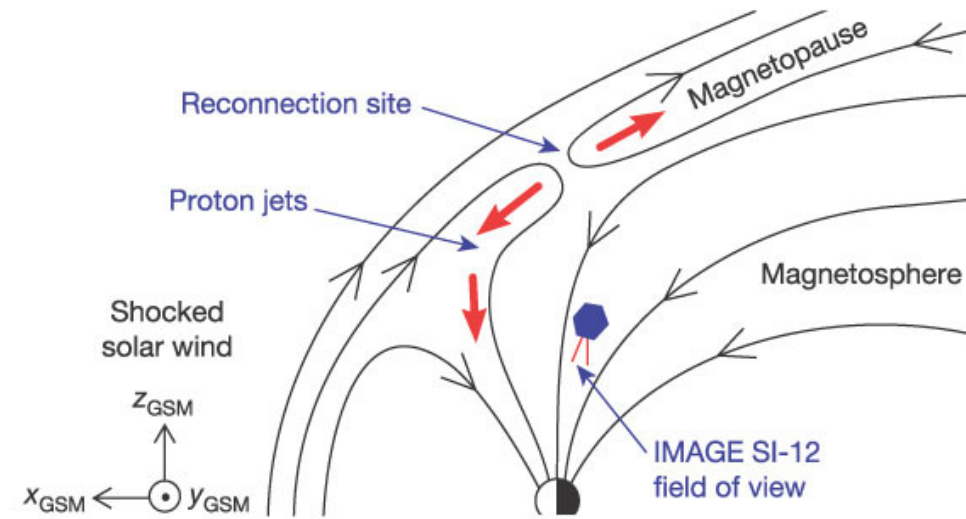
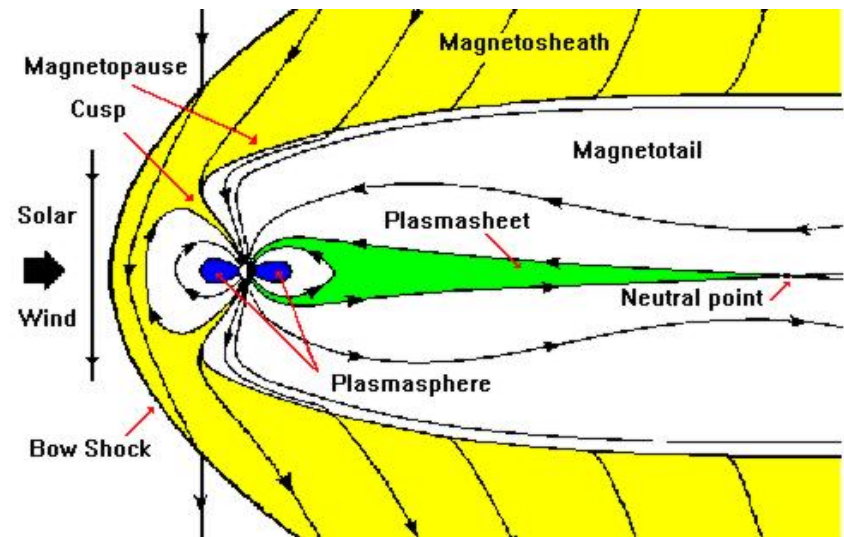
- ① Motivation: model space weather and fast reconnection
- ② Problem: efficient plasma simulation for multiple scales
- ③ Strategy: domain decomposition
- ④ 1-D simulations



Physical motivation: Space weather

Broad goal: to model **space weather**.

- Earth bombarded with **solar wind**.
- Solar wind is generally deflected by Earth's magnetic field.
- Reconnection of magnetic field lines allows plasma to enter the region occupied by Earth's magnetic field lines and propagate to Earth's poles.



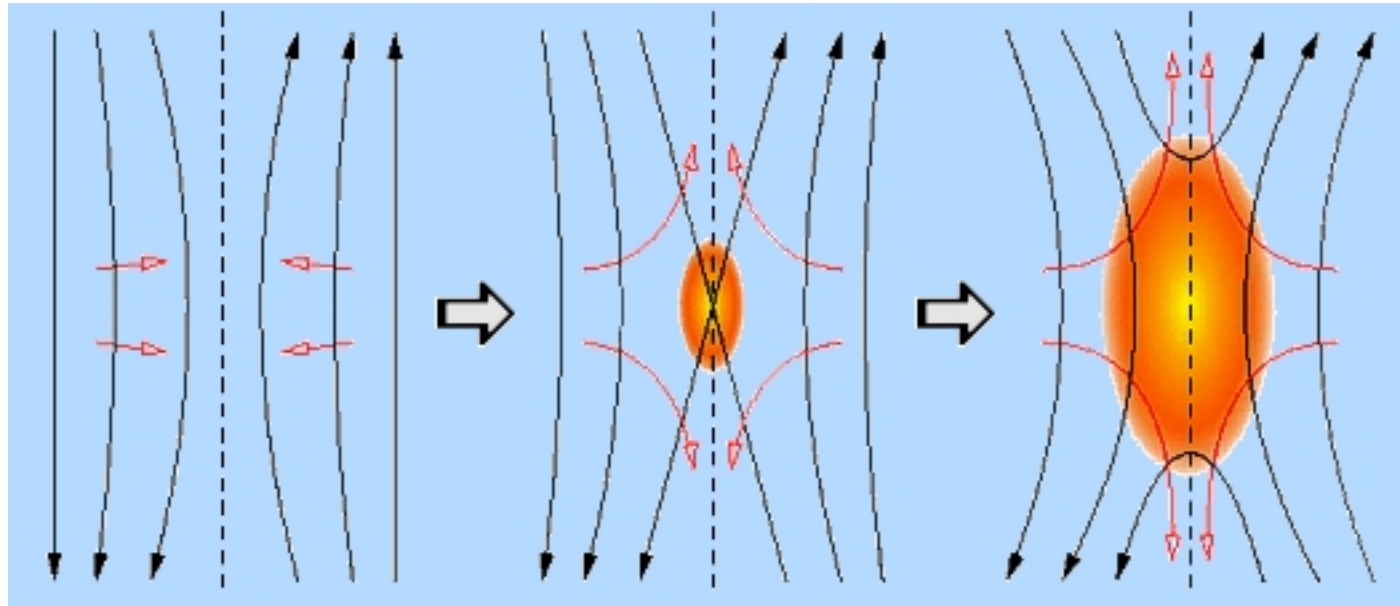
From *Continuous magnetic reconnection at Earth's magnetopause*,
H. U. Frey, T. D. Phan, S. A. Fuselier and S. B. Mende,

Nature 426, 533-537(4 December 2003)



Critical phenomenon: fast magnetic reconnection _____

Fast reconnection provides the mechanism that allows solar storms to trigger violent geomagnetic storms.



http://www.aldebaran.cz/astrofizika/plazma/reconnection_en.html

Our project is to develop an efficient algorithm that resolves **fast magnetic reconnection**.



Simulating fast reconnection: a multiscale problem ---

Fast reconnection makes space plasma simulation a multiscale problem.

- ① Finest model: Collisionless Kinetic (PIC: particle-in-cell)
 - computationally expensive; PIC is noisy
 - admits fast reconnection and gets right structure of reconnection region

- ② Fine model: ideal 2-fluid
 - computationally expensive
 - admits fast reconnection
 - agrees with collisionless PIC for low plasma β .

- ③ Coarse model: MHD (magnetohydrodynamics)
 - computationally cheap
 - adequate for most of the domain
 - ideal MHD does not admit reconnection
 - resistive MHD does not admit fast reconnection



Strategy: domain-decomposition ---

We want to develop a domain-decomposition multiscale algorithm which uses a kinetic model in small regions where reconnection is occurring and elsewhere uses MHD.

Why stitching models is a good idea:

- 2-fluid converges to MHD as gyroradius goes to zero
- ratio of explicit 2-fluid/PIC to MHD cost increases with inverse square of nondimensionalized gyroradius



Strategy for a stitched model ---

Framework of the domain-decomposition (“stitching”) model we are working towards:

- use MHD solver over the global domain
- use embedded microscale (2-fluid/PIC) solver in regions where conditions are hospitable to fast reconnection

How data exchange should work:

- MHD provides microscale solver with boundary data
- microscale 2-fluid provides MHD with corrected values in overlap region.
- stitch smoothly at the boundary between models using a “sponge layer”



Model state variables

Exchanging data requires specifying the state variables of each model (and the maps between them.)

MHD state variables:

$$\begin{pmatrix} \rho \\ \rho \mathbf{u} \\ \mathcal{E} \\ \mathbf{B} \end{pmatrix} = \begin{pmatrix} \text{mass} \\ \text{momentum} \\ \text{energy} \\ \text{magnetic field} \end{pmatrix}$$

PIC state variables:

$$\begin{pmatrix} \mathbf{B} \\ \mathbf{E} \\ (\mathbf{x}_p)_{p=1}^N \\ (\mathbf{v}_p)_{p=1}^N \end{pmatrix} = \begin{pmatrix} \text{electric field} \\ \text{magnetic field} \\ \text{particle positions} \\ \text{particle velocities} \end{pmatrix}$$

2-fluid state variables:

$$\begin{pmatrix} \rho_i \\ \rho_i \mathbf{u}_i \\ \mathcal{E}_i \\ \rho_e \\ \rho_e \mathbf{u}_e \\ \mathcal{E}_e \\ \mathbf{B} \\ \mathbf{E} \end{pmatrix} = \begin{pmatrix} \text{ion mass} \\ \text{ion momentum} \\ \text{ion energy} \\ \text{electron mass} \\ \text{electron momentum} \\ \text{electron energy} \\ \text{magnetic field} \\ \text{electric field} \end{pmatrix}$$



Mapping between micro and macro states ---

- Mapping from micro to macro states is called *compression*.
- Mapping from macro to micro states is called *reconstruction*.
- Compression: typically involves straightforward summing or averaging
- Reconstruction: the inverse mapping is nonunique, so reconstruction requires additional assumptions or information to pick out a solution.



Mapping from 2-fluid to MHD states

A natural mapping from MHD to 2-fluid states (compression) is:

$$\rho = \rho_i + \rho_e$$

$$\rho \mathbf{u} = \rho_i \mathbf{u}_i + \rho_e \mathbf{u}_e$$

$$\mathcal{E} = \mathcal{E}_i + \mathcal{E}_e$$

$$\mathbf{B} = \mathbf{B}$$

(This regards species drift velocity as part of the thermal energy in MHD.)

However, to avoid the danger of computing negative pressures, we abandon energy conservation and instead sum pressure (i.e. thermal energy):

$$\rho = \rho_i + \rho_e$$

$$\rho \mathbf{u} = \rho_i \mathbf{u}_i + \rho_e \mathbf{u}_e$$

$$p = p_i + p_e$$

$$\mathbf{B} = \mathbf{B}$$



Reconstructing 2-fluid from MHD states

To invert the compression mapping we need additional information:

- ① *ratio of number densities*: provided by MHD assumption of quasineutrality:

$$\rho_i = \frac{m_i}{m_i + m_e} \rho, \quad \rho_e = \frac{m_e}{m_i + m_e} \rho.$$

- ② *drift velocities*: provided by MHD assumptions of quasineutrality and $\partial_t \mathbf{E} \approx 0$ (Ampere's law):

$$\mathbf{J} = \mu_0^{-1} \nabla \times \mathbf{B},$$

$$\mathbf{u}_i = \mathbf{u} + \frac{m_e}{e\rho} \mathbf{J}, \quad \mathbf{u}_e = \mathbf{u} - \frac{m_i}{e\rho} \mathbf{J}.$$

- ③ *ratio of thermal energies*: used to split thermal energy (typically we split pressure instead to avoid negative pressures):

$$p_i = \frac{T_i}{T_i + T_e} p, \quad p_e = \frac{T_e}{T_i + T_e} p$$



Mapping between kinetic and 2-fluid states ---

- ① Compression mapping from kinetic to 2-fluid states:
 - compute statistical moments for each cell to get values of mass, momentum, and pressure or energy.

- ② Reconstruction of particles from moments:
 - uses moments and assumed form of distribution of velocities (e.g. Maxwellian)
 - needed when creating particles for an initial state or injecting particles at model boundaries.



Equations: Vlasov

We take the Vlasov equation as the true description of a collisionless plasma. It says that the particle density of each species is conserved in phase space.

$$\partial_t f_s + \nabla_{\mathbf{x}} \cdot (\mathbf{v} f_s) + \nabla_{\mathbf{v}} \cdot \left(\frac{q_s}{m_s} (\mathbf{E} + \mathbf{v} \times \mathbf{B}) f_s \right) = 0,$$

Here s is a species index, $f_s(t, \mathbf{x}, \mathbf{v})$ is particle density as a function of the independent variables.



Equations: kinetic ---

The equations of the kinetic model are Maxwell's equations and the Lorentz force to govern particle motion:

$$\partial_t \mathbf{B} = -\nabla \times E, \quad \nabla \cdot \mathbf{B} = 0,$$

$$\partial_t \mathbf{E} = c^2 \nabla \times B - \mathbf{J}/\epsilon, \quad \nabla \cdot \mathbf{E} = \sigma,$$

$$\partial_t(\gamma \mathbf{v}_p) = \frac{1}{r} \frac{q_p}{m_p} \left(\mathbf{E}(\mathbf{x}_p) + \mathbf{v}_p \times \mathbf{B}(\mathbf{x}_p) \right), \quad \partial_t \mathbf{x}_p = \mathbf{v}_p,$$

$$\mathbf{J} = \sum_p q_p \mathbf{v}_p S,$$

where p denotes particle index and S denotes the spatial charge distribution of a single particle (e.g. an impulse function). (In the nondimensionalization r is the nondimensionalized gyroradius of a typical ion.)



Equations: 2-fluid

The equations of the ideal 2-fluid model are Maxwell's equations coupled to the ideal gas equations for each species (with no direct coupling between species):

$$\partial_t \begin{bmatrix} \rho_i \\ \rho_e \\ \rho_i \mathbf{u}_i \\ \rho_e \mathbf{u}_e \\ \mathcal{E}_i \\ \mathcal{E}_e \end{bmatrix} + \nabla \cdot \begin{bmatrix} \rho_i \mathbf{u}_i \\ \rho_e \mathbf{u}_e \\ \rho_i \mathbf{u}_i \mathbf{u}_i + p_i \mathbb{I} \\ \rho_e \mathbf{u}_e \mathbf{u}_e + p_e \mathbb{I} \\ \mathbf{u}_i \mathcal{E}_i + \mathbf{u}_i p_i \\ \mathbf{u}_e \mathcal{E}_e + \mathbf{u}_e p_e \end{bmatrix} = \frac{1}{r} \begin{bmatrix} 0 \\ 0 \\ \sigma_i \mathbf{E} + \mathbf{J}_i \times \mathbf{B} \\ \sigma_e \mathbf{E} + \mathbf{J}_e \times \mathbf{B} \\ \mathbf{J}_i \cdot \mathbf{E} \\ \mathbf{J}_e \cdot \mathbf{E} \end{bmatrix}$$

$$\begin{aligned} \partial_t \mathbf{B} + \nabla \times \mathbf{E} &= 0, & \nabla \cdot \mathbf{B} &= 0, \\ \partial_t \mathbf{E} - c^2 \nabla \times \mathbf{B} &= -\mathbf{J}/\epsilon, & \nabla \cdot \mathbf{E} &= \sigma/\epsilon. \end{aligned}$$

Here $r := \frac{v_0 m_0}{x_0 q_0 B_0} = r_L/x_0$ is a nondimensionalized gyroradius and $\epsilon = \frac{\epsilon_0 v_0 B_0}{q_0 n_0 x_0}$ is a fake permittivity; we can write $\epsilon = r \lambda^2$, where $\lambda^2 := \frac{\epsilon_0 B_0 v_0}{q_0 n_0 x_0}$ defines the ratio of the Debye length

$\lambda_D := \sqrt{\left(\frac{\epsilon_0 m_0 v_0^2}{n_0 q_0^2}\right)}$ to the gyroradius.



Equations: MHD

The equations of ideal MHD in conservative form are

$$\partial_t \begin{bmatrix} \rho \\ \rho \mathbf{u} \\ \tilde{\mathcal{E}} \\ \mathbf{B} \end{bmatrix} + \nabla \cdot \begin{bmatrix} \rho \mathbf{u} \\ \rho \mathbf{u} \mathbf{u} + \mathbb{I} \tilde{p}_{\text{MHD}} - \mu_0^{-1} (\mathbf{B} \mathbf{B}) \\ \mathbf{u} (\tilde{\mathcal{E}} + \tilde{p}_{\text{MHD}}) - \mu_0^{-1} \mathbf{B} \mathbf{B} \cdot \mathbf{u} \\ \mathbf{u} \mathbf{B} - \mathbf{B} \mathbf{u} \end{bmatrix} = 0,$$

where $\tilde{\mathcal{E}} = \mathcal{E} + \mu_0^{-1} B^2/2$ is total energy, where $\mathcal{E} = (3/2)p_{\text{MHD}} + (1/2)\rho u^2$ is MHD gas energy, and $\tilde{p}_{\text{MHD}} = p_{\text{MHD}} + \mu_0^{-1} B^2/2$ is total pressure.



Numerical schemes

We have implemented second-order-accurate time-splitting finite-volume schemes that maintain Maxwell's divergence constraints for each of the three models. The MHD and 2-fluid schemes are conservative and apply shock-capturing limiters.



Numerical PIC scheme

Our PIC scheme uses staggering in time and space to achieve second-order accuracy and maintain the divergence constraints. Our scheme is:

$$(\partial_t \mathbf{E})^{m+1/2} = c^2 (\nabla \times \mathbf{B})^{m+1/2} - \mathbf{J}^{n+1/2} / \epsilon,$$

$$\text{implicit case: } (\partial_t \mathbf{B})^{m+1/2} = -(\nabla \times \mathbf{E})^{m+1/2}$$

$$\text{explicit case: } (\partial_t \mathbf{B})^{m+1} = -(\nabla \times \mathbf{E})^{m+1}$$

$$(\partial_t (\gamma \mathbf{v})_p)^n = \frac{1}{r} \frac{q_p}{m_p} \left(\mathbf{E}^n(\mathbf{x}_p^n) + \frac{\mathbf{v}_p^{n+1/2} + \mathbf{v}_p^{n-1/2}}{2} \times \mathbf{B}^n(\mathbf{x}_p^n) \right),$$

$$(\partial_t \mathbf{x}_p)^{n+1/2} = \mathbf{v}_p^{n+1/2}, \quad \mathbf{J}^{n+1/2} = \sum_p q_p \mathbf{v}_p^{n+1/2} S.$$

For second-order accuracy we chose the particle shape S to be the size of a mesh cell.

The discrete differential operators denote second-order centered difference operators in time and space. The spatial staggering (Yee scheme) centers vector components on the cell faces to which they are perpendicular and centers components of pseudovectors (e.g. \mathbf{B}) along cell edges. Taking the discrete divergence of the electromagnetic evolution equations shows that $\nabla \cdot \mathbf{B} = 0$ is maintained and that $(\nabla \cdot \mathbf{E})^n = \sigma^n / \epsilon$ is maintained if we enforce that current is charge flux, i.e., $(\partial_t \sigma)^{n+1/2} + \mathbf{J}^{n+1/2} = 0$.



Numerical MHD scheme

The ideal MHD system is hyperbolic, so we used a finite-volume shock-capturing method based on the eigenstructure of the flux jacobian.

Remark: It is easier to find the eigenstructure for primitive variables and then transform to conserved variables. The 1-D MHD equations in primitive variables and quasilinear form are:

$$\begin{pmatrix} \rho \\ u_1 \\ u_2 \\ u_3 \\ p \\ B_2 \\ B_3 \end{pmatrix}_t + \begin{bmatrix} u_1 & \rho & 0 & 0 & 0 & 0 & 0 \\ 0 & u_1 & 0 & 0 & \frac{1}{\mu_0 \rho} & \frac{B_2}{\mu_0 \rho} & \frac{B_3}{\mu_0 \rho} \\ 0 & 0 & u_1 & 0 & 0 & \frac{-B_1}{\mu_0 \rho} & 0 \\ 0 & 0 & 0 & u_1 & 0 & 0 & \frac{-B_1}{\mu_0 \rho} \\ 0 & \gamma p & 0 & 0 & u_1 & 0 & 0 \\ 0 & B_2 & -B_1 & 0 & 0 & u_1 & 0 \\ 0 & B_3 & 0 & -B_1 & 0 & 0 & u_1 \end{bmatrix} \cdot \begin{pmatrix} \rho \\ u_1 \\ u_2 \\ u_3 \\ p \\ B_2 \\ B_3 \end{pmatrix}_x = 0$$



Numerical 2-fluid scheme ---

For the two-fluid solver, we used time-splitting to decouple the hyperbolic flux from the (nondifferentiated) source term. We used a finite-volume shock-capturing method for the hyperbolic flux and RK4 for the source term ODE.



Preliminary studies

The need to design a stitched model has prompted us to carry out some preliminary studies.

- need to show that waves are transmitted smoothly across the stitching layer between model boundaries
- need to study convergence of microscale model to macroscale model to determine where to use the macroscale versus microscale model.



1D convergence studies

We have done 1D convergence studies for the

- ① MHD,
- ② 2-fluid, and
- ③ PIC

models for the following problems:

- Brio-Wu shock problem
- polarized Alfvén waves
- Magnetosonic waves



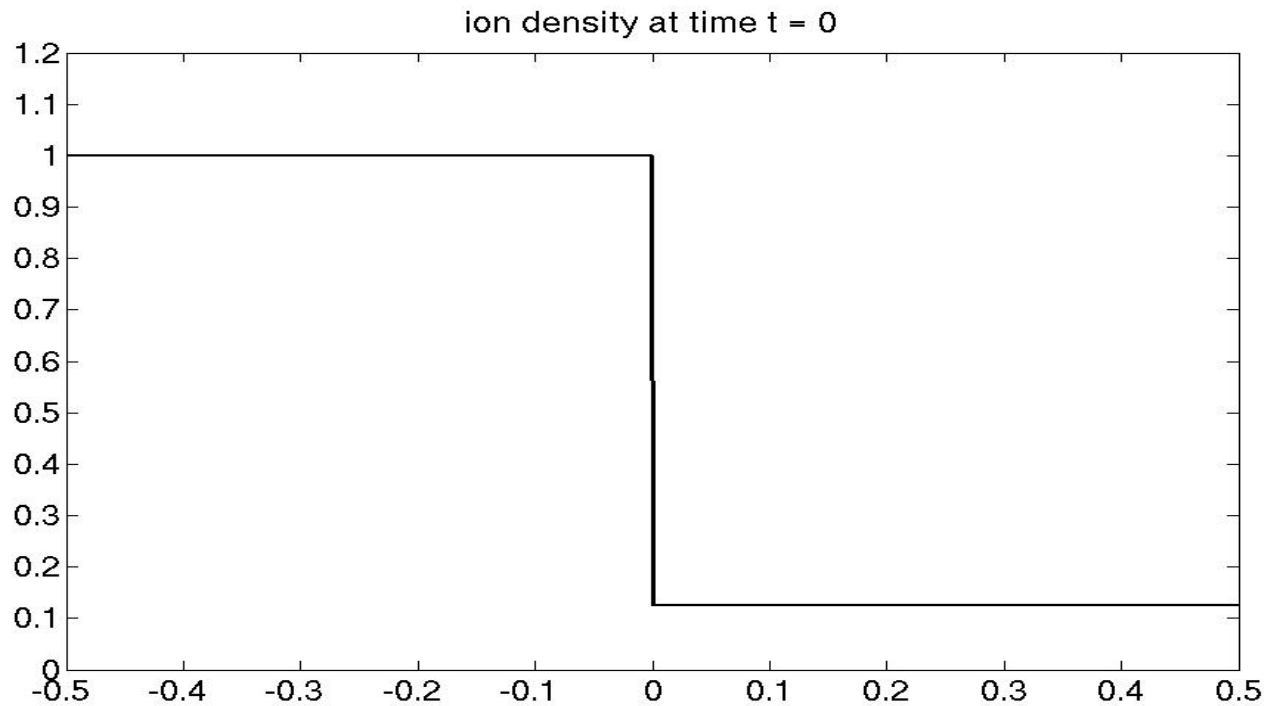
Brio-Wu shock problem results ---

- For a large light speed, as gyroradius goes to zero, the 2-fluid simulation seem to weakly converge to a limit that is close to the 1-fluid simulation.
- PIC simulations show rough agreement with 2-fluid simulations as we increase the number of particles



Computations: Brio-Wu shock problem

We computed solutions to the Brio-Wu 1-dimensional shock problem [?].



Initial conditions for ion density:
discontinuity at zero, elsewhere constant.



Computations: Brio-Wu shock problem

For **MHD** the Brio-Wu initial conditions to the left and right of zero are:

$$\begin{bmatrix} \rho \\ v_1 \\ v_2 \\ v_3 \\ p \\ B^1 \\ B^2 \\ B^3 \end{bmatrix}_{\text{left}} = \begin{bmatrix} 1.0 \\ 0 \\ 0 \\ 0 \\ 1.0 \\ 0.75 \\ 1.0 \\ 0 \end{bmatrix} \quad \text{and} \quad \begin{bmatrix} \rho \\ v_1 \\ v_2 \\ v_3 \\ p \\ B^1 \\ B^2 \\ B^3 \end{bmatrix}_{\text{right}} = \begin{bmatrix} 0.125 \\ 0 \\ 0 \\ 0 \\ 0.1 \\ 0.75 \\ -1.0 \\ 0 \end{bmatrix}$$

The equivalent **two-fluid** initial conditions are:

$$\begin{bmatrix} \rho_i \\ v_i^1 \\ v_i^2 \\ v_i^3 \\ v_i \\ p_i \\ \rho_e \\ v_e^1 \\ v_e^2 \\ v_e^3 \\ v_e \\ p_e \\ B^1 \\ B^2 \\ B^3 \\ E^1 \\ E^2 \\ E^3 \end{bmatrix}_{\text{left}} = \begin{bmatrix} 1.0 \\ 0 \\ 0 \\ 0 \\ 0 \\ 0.5 \\ 1.0 \frac{m_e}{m_i} \\ 0 \\ 0 \\ 0 \\ 0 \\ 0 \\ 0.5 \\ 0.75 \\ 1.0 \\ 0 \\ 0 \\ 0 \\ 0 \end{bmatrix} \quad \text{and} \quad \begin{bmatrix} \rho_i \\ v_i^1 \\ v_i^2 \\ v_i^3 \\ v_i \\ p_i \\ \rho_e \\ v_e^1 \\ v_e^2 \\ v_e^3 \\ v_e \\ p_e \\ B^1 \\ B^2 \\ B^3 \\ E^1 \\ E^2 \\ E^3 \end{bmatrix}_{\text{right}} = \begin{bmatrix} 0.125 \\ 0 \\ 0 \\ 0 \\ 0 \\ 0.05 \\ 0.125 \frac{m_e}{m_i} \\ 0 \\ 0 \\ 0 \\ 0 \\ 0 \\ 0.05 \\ 0.75 \\ -1.0 \\ 0 \\ 0 \\ 0 \\ 0 \end{bmatrix}$$



Computations

We plotted ion density at nondimensionalized time $t = 0.1$ for a range of values of the nondimensionalized Larmor radius:

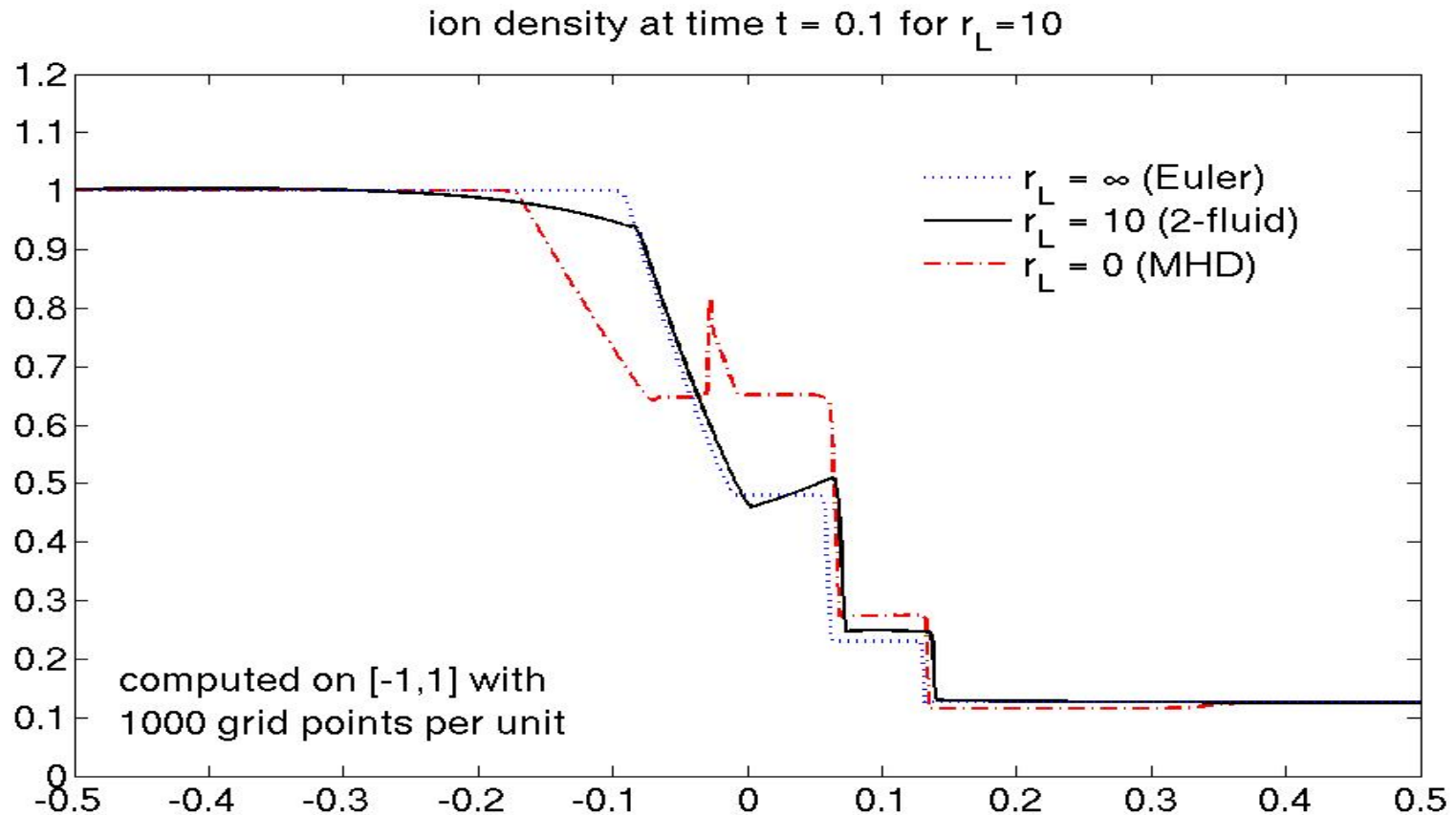
- $r_L = \infty$ (an Euler gas dynamics computation),
- $r_L = 10, 1, 0.1, 0.01, 0.003$ (two-fluid computations), and
- $r_L = 0$ (an ideal MHD computation).

Results:

- As $r_L \rightarrow 0$, the solution seems to weakly approach the MHD solution.
- For smaller values of r_L computation becomes prohibitively expensive as we need a finer computational grid to prevent negative pressures or densities from crashing the code and to get convergence.
- For intermediate values of r_L , the computational domain needs to be extended the most due to substantial fast-moving oscillations.



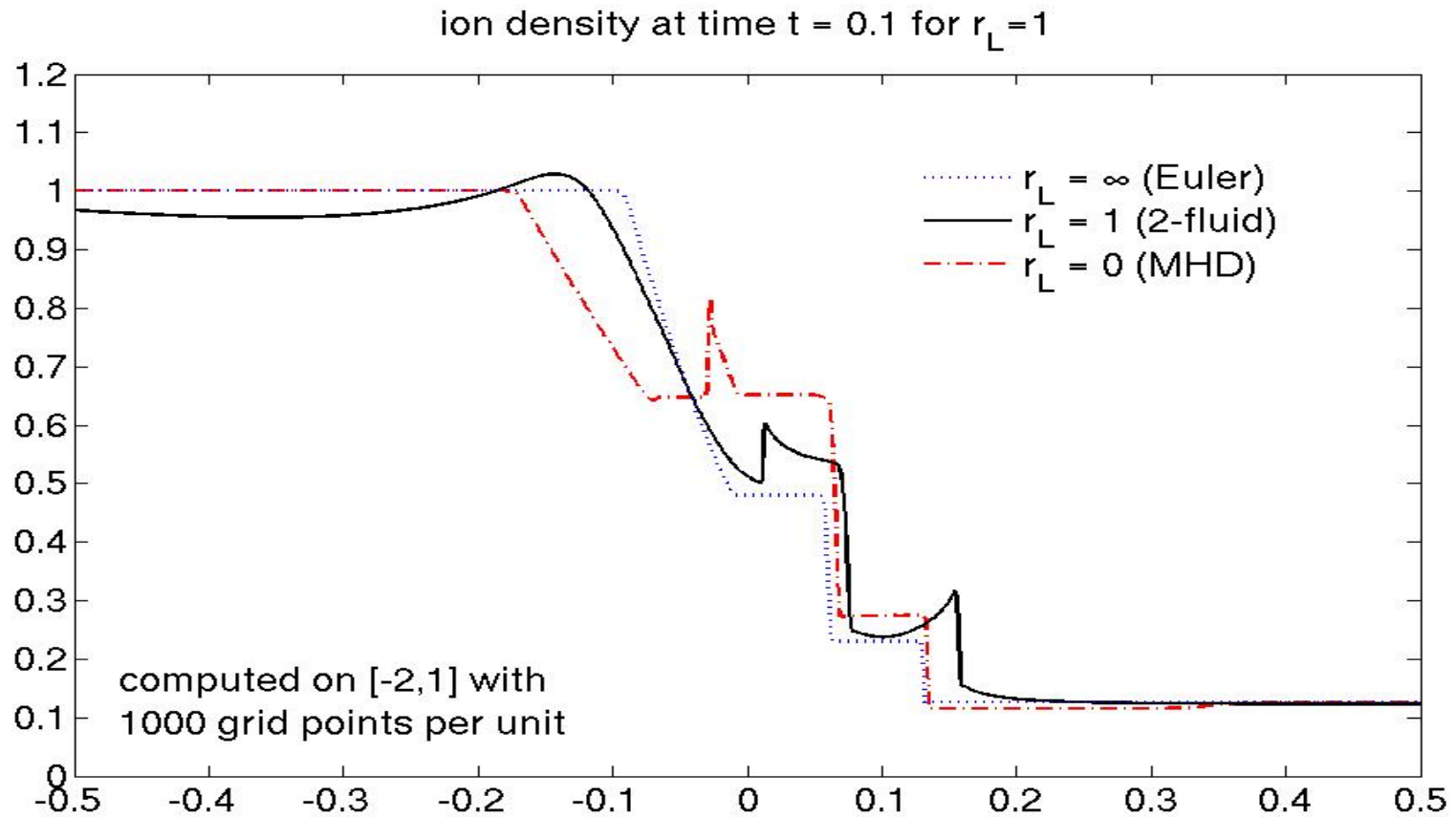
Computations (cell-centered), $r_L = 10$



When the Larmor radius is large ($r_L = 10$), the electromagnetic effects are weak and the ions behave like an ideal gas. (At $r_L = 100$, 2-fluid is indistinguishable from Euler.)



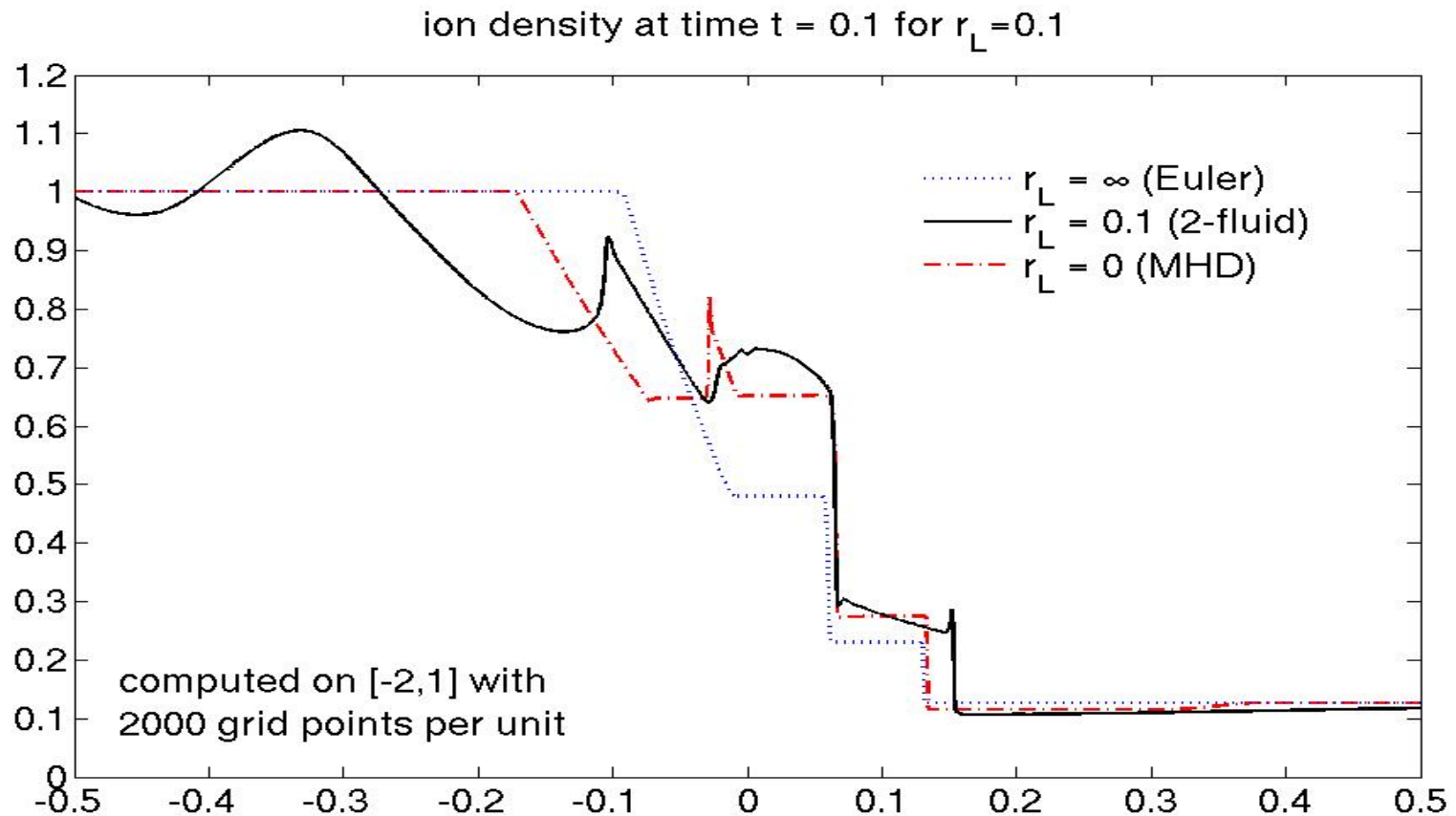
Computations (cell-centered), $r_L = 1$



As we decrease the Larmor radius, the solution begins to transition away from gas dynamics (and eventually toward MHD).



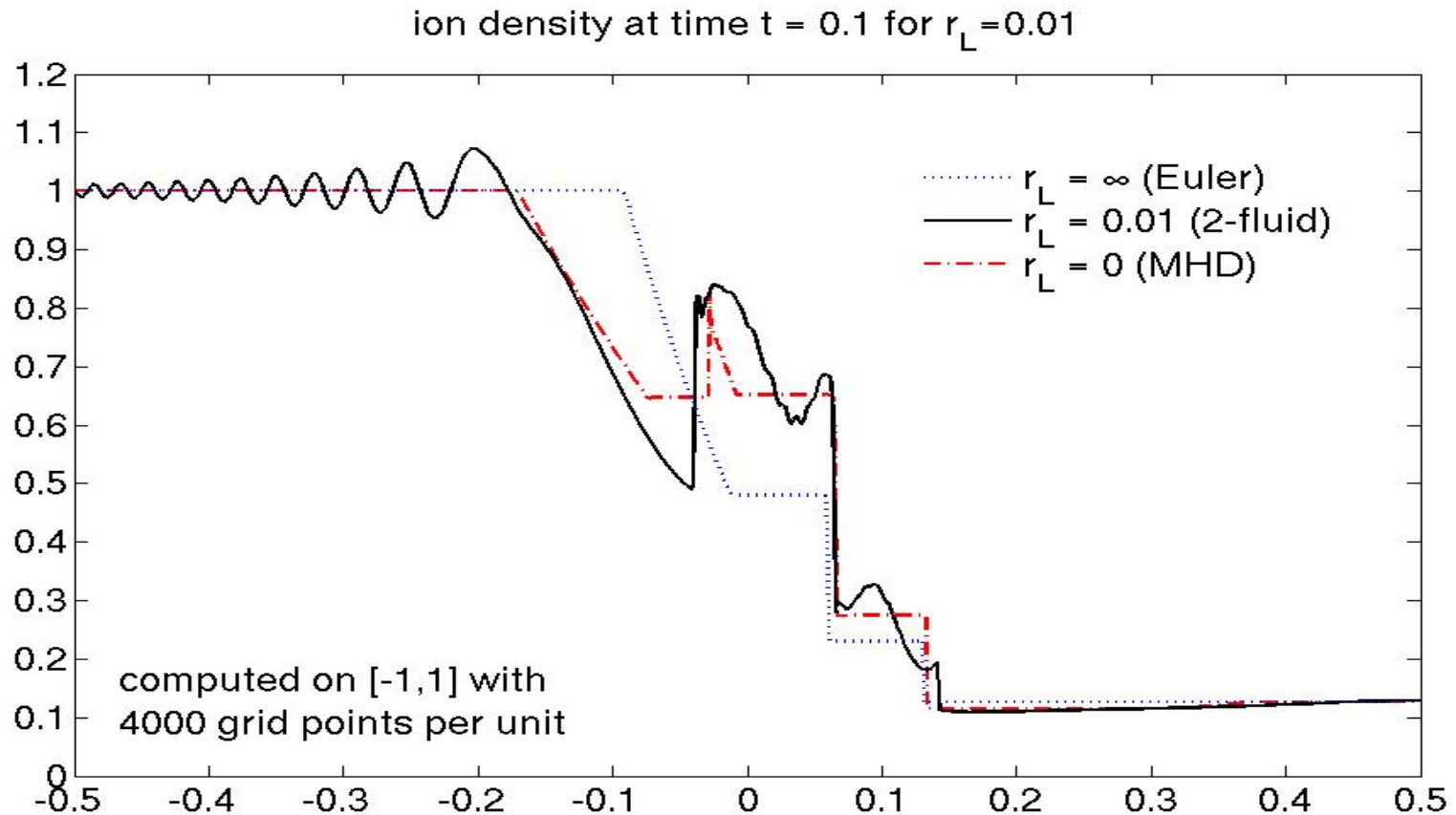
Computations (cell-centered), $r_L = 0.1$



When $t \approx r_L$, the solution is roughly intermediate between Euler and MHD.



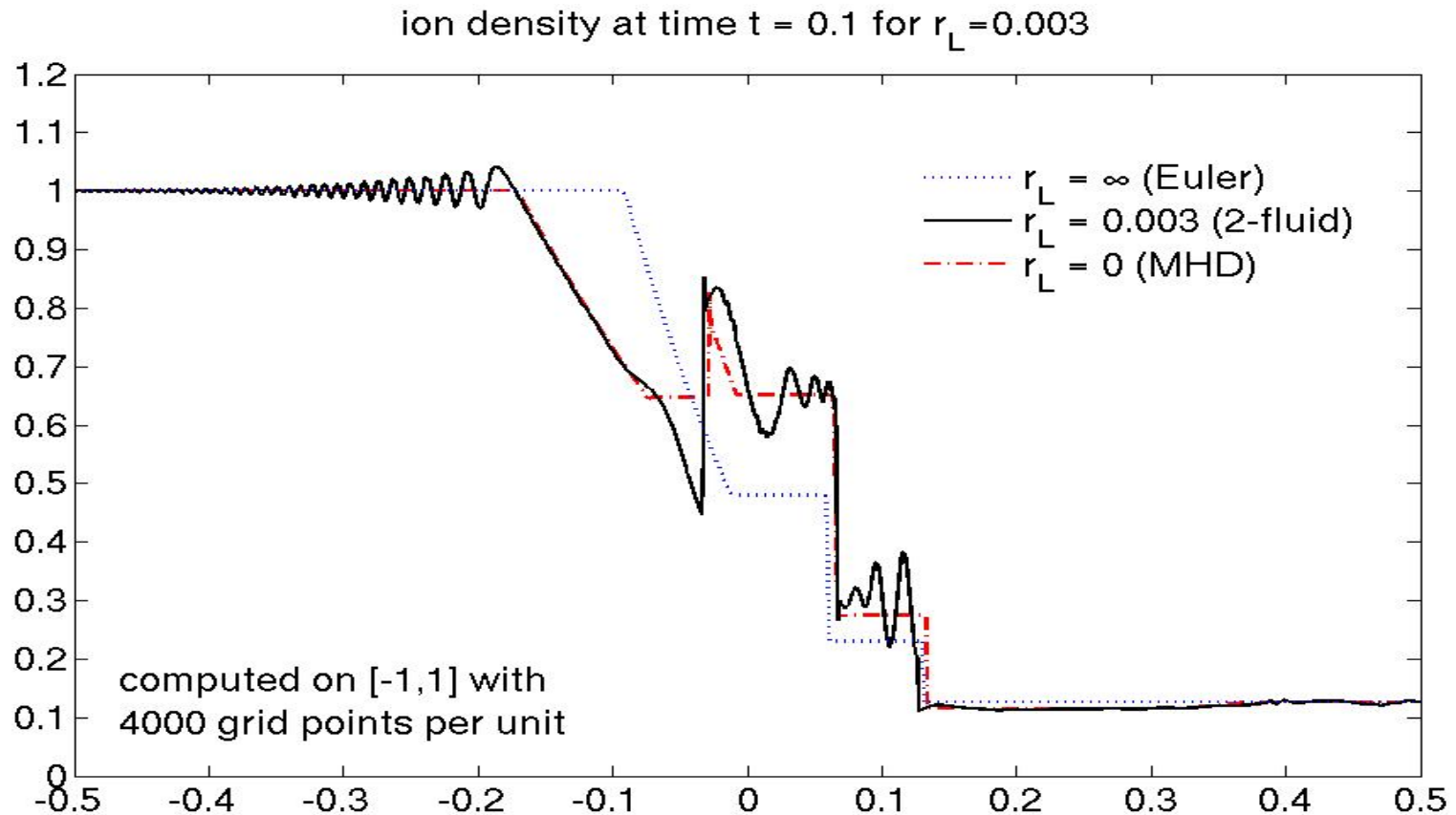
Computations (cell-centered), $r_L = 0.01$



As the Larmor radius becomes even smaller, the frequency of the oscillations increases and the solution begins to weakly approach the MHD solution.



Computations (cell-centered), $r_L = 0.003$



Convergence to MHD is suggested but far from confirmed. Unfortunately, computational expense increases with decreasing Larmor radius.



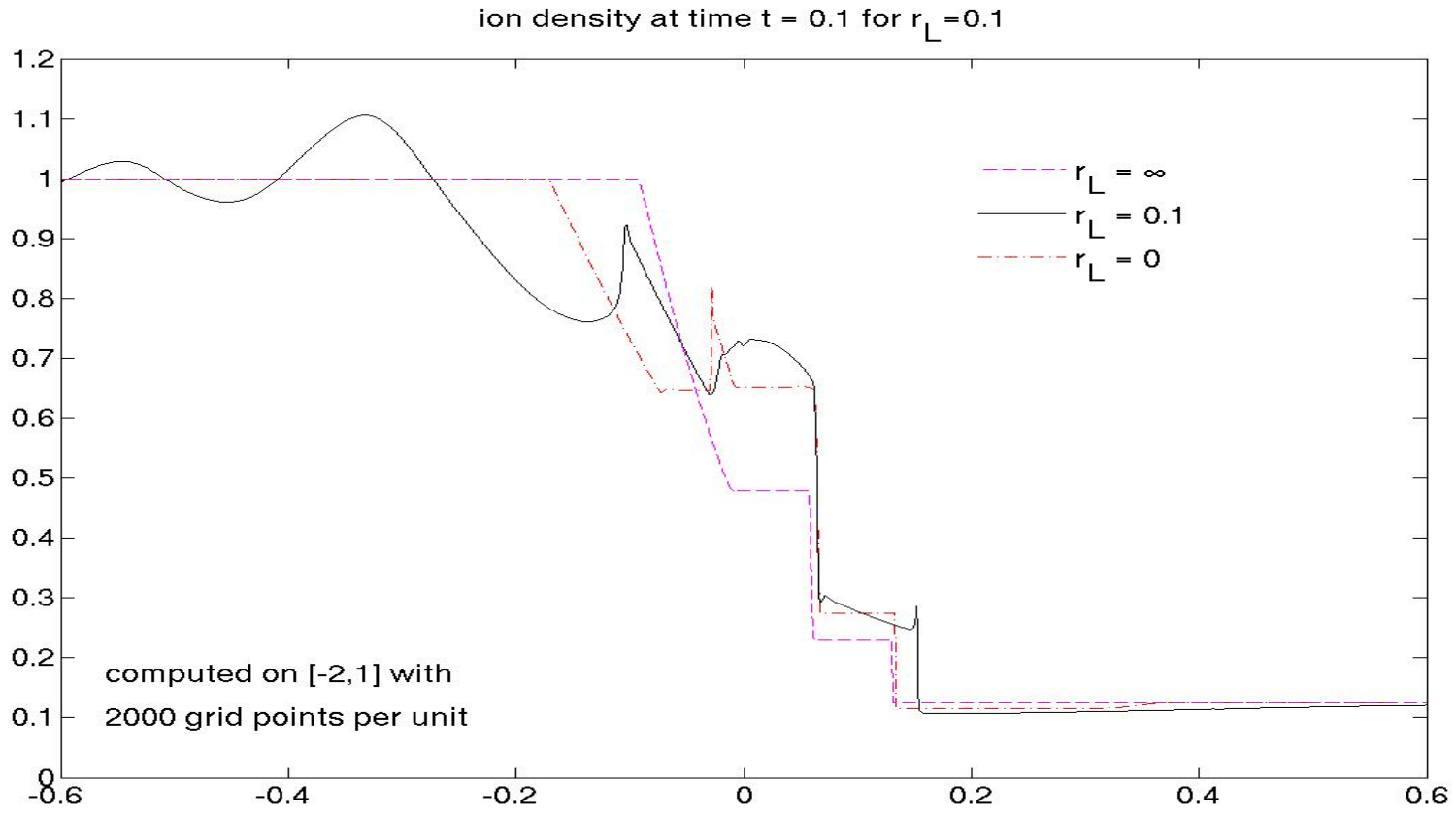
Computations with Yee scheme

Results:

- For large Larmor radius the Yee scheme was indistinguishable from the cell-centered scheme.
- For intermediate values of Larmor radius ($r_L = t = 0.1$), the Yee scheme is less accurate for a coarse mesh but more accurate for a fine mesh.
- For small Larmor radius the Yee scheme required a prohibitively small mesh size to prevent negative or vanishing densities.
- Suggested conclusion: Use the cell-centered scheme for a large mesh and switch to the Yee scheme for a sufficiently fine mesh.



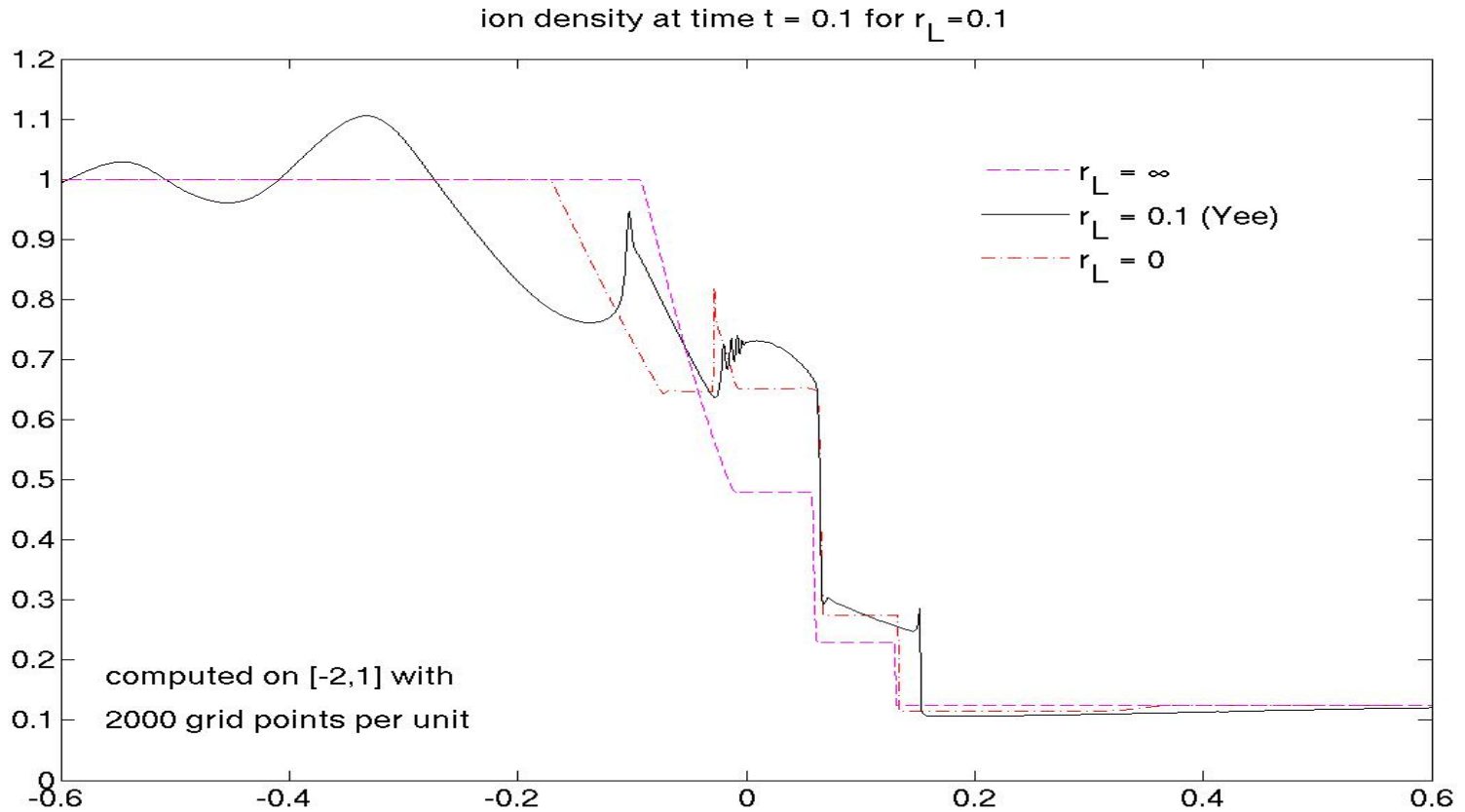
Computations, cell-centered, $r_L = 0.1$



(Cell-centered computation for comparison with Yee scheme.)



Computations: Comparison with Yee scheme, $r_L = 0.1$ ---

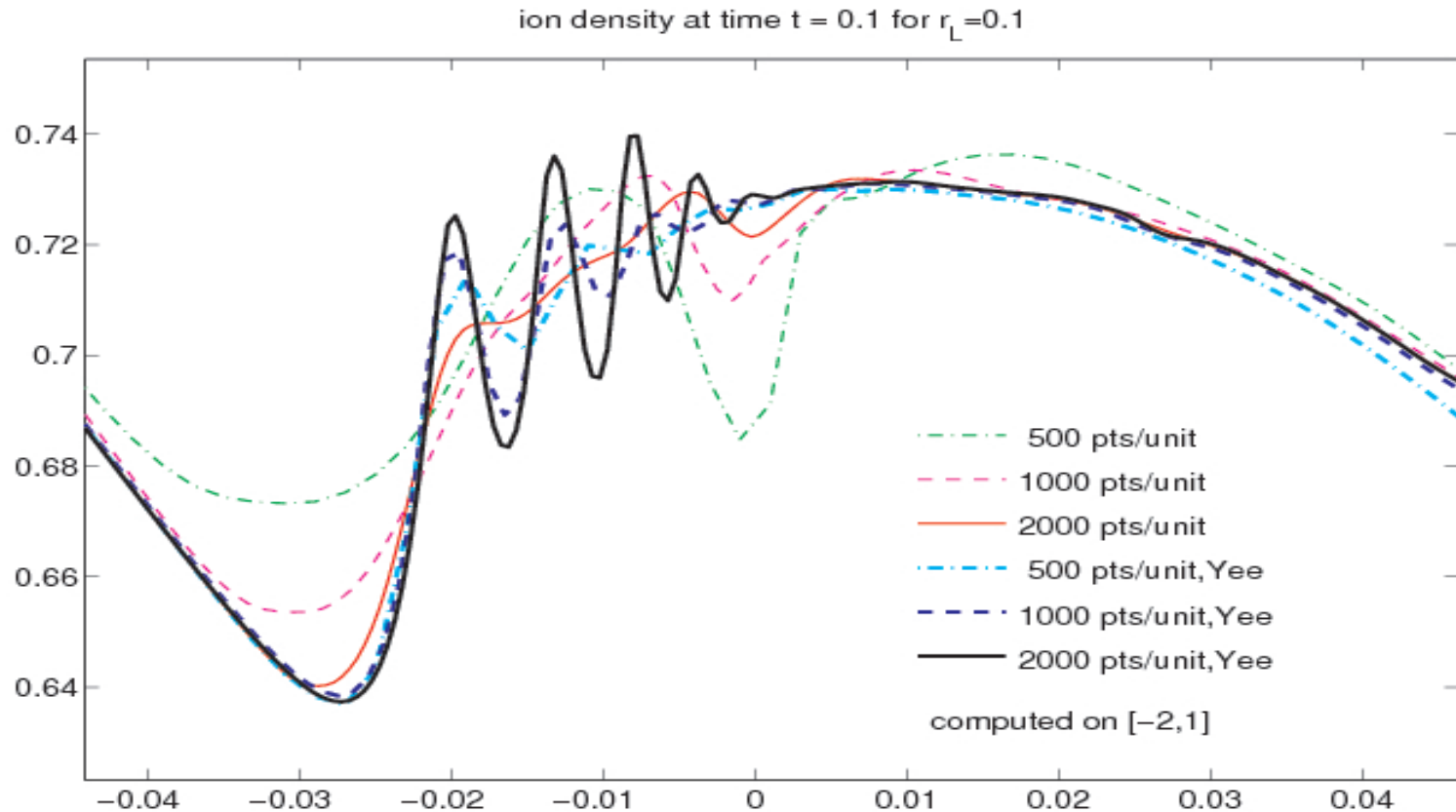


The plot of the Yee scheme is indistinguishable from the unstaggered scheme except in the squiggly area near the right end of the slow compound wave of MHD and the peak in the rarefaction wave of MHD.



Computations: Comparison with Yee scheme, $r_L = 0.1$ _____

Close-up near MHD compound wave.

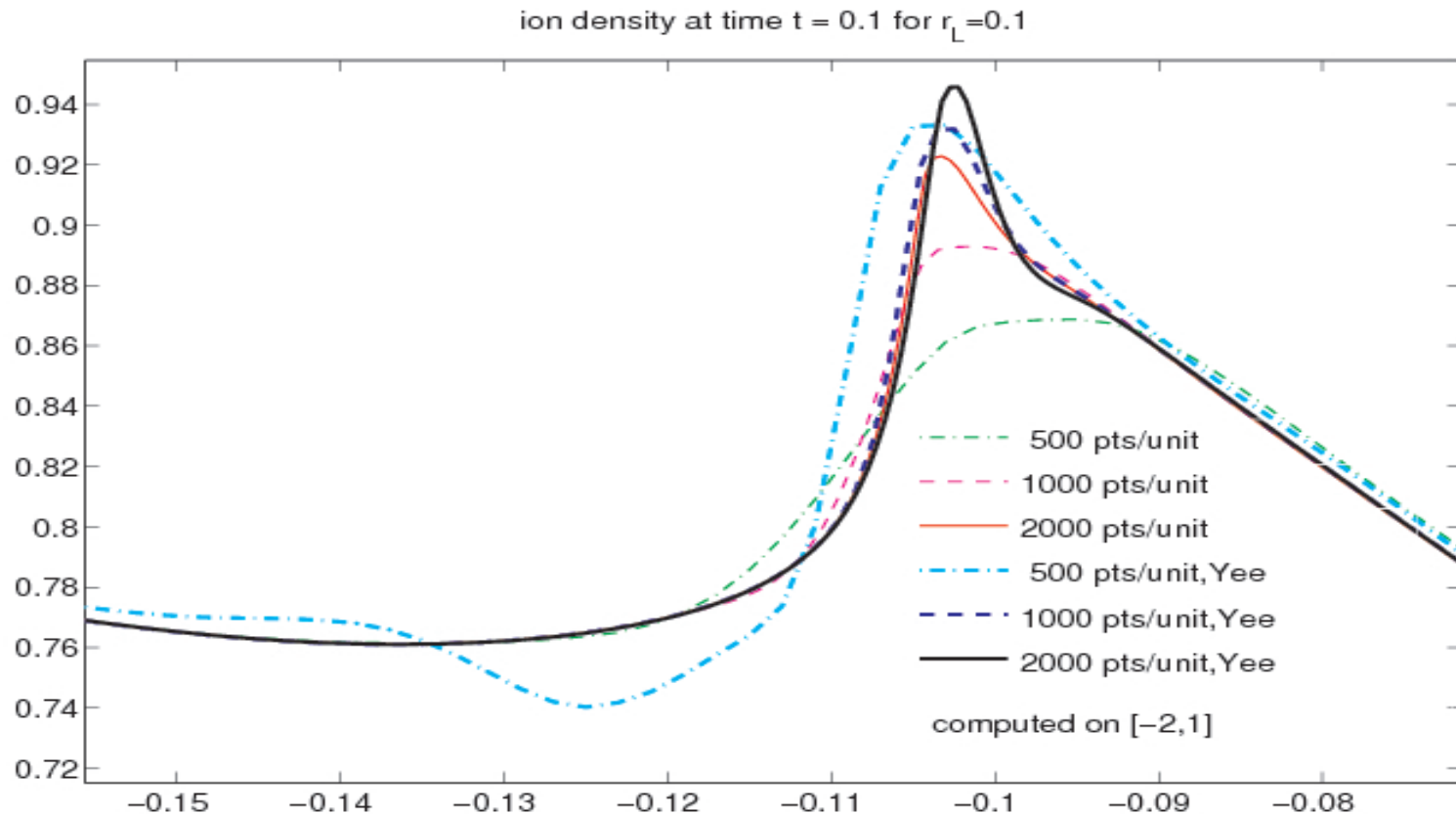


The Yee scheme converges much more rapidly in this region of high oscillation near the right end of the slow compound wave of MHD (compare the highly resolved solution in Fig. 4 of [?]).



Computations: Comparison with Yee scheme, $r_L = 0.1$ _____

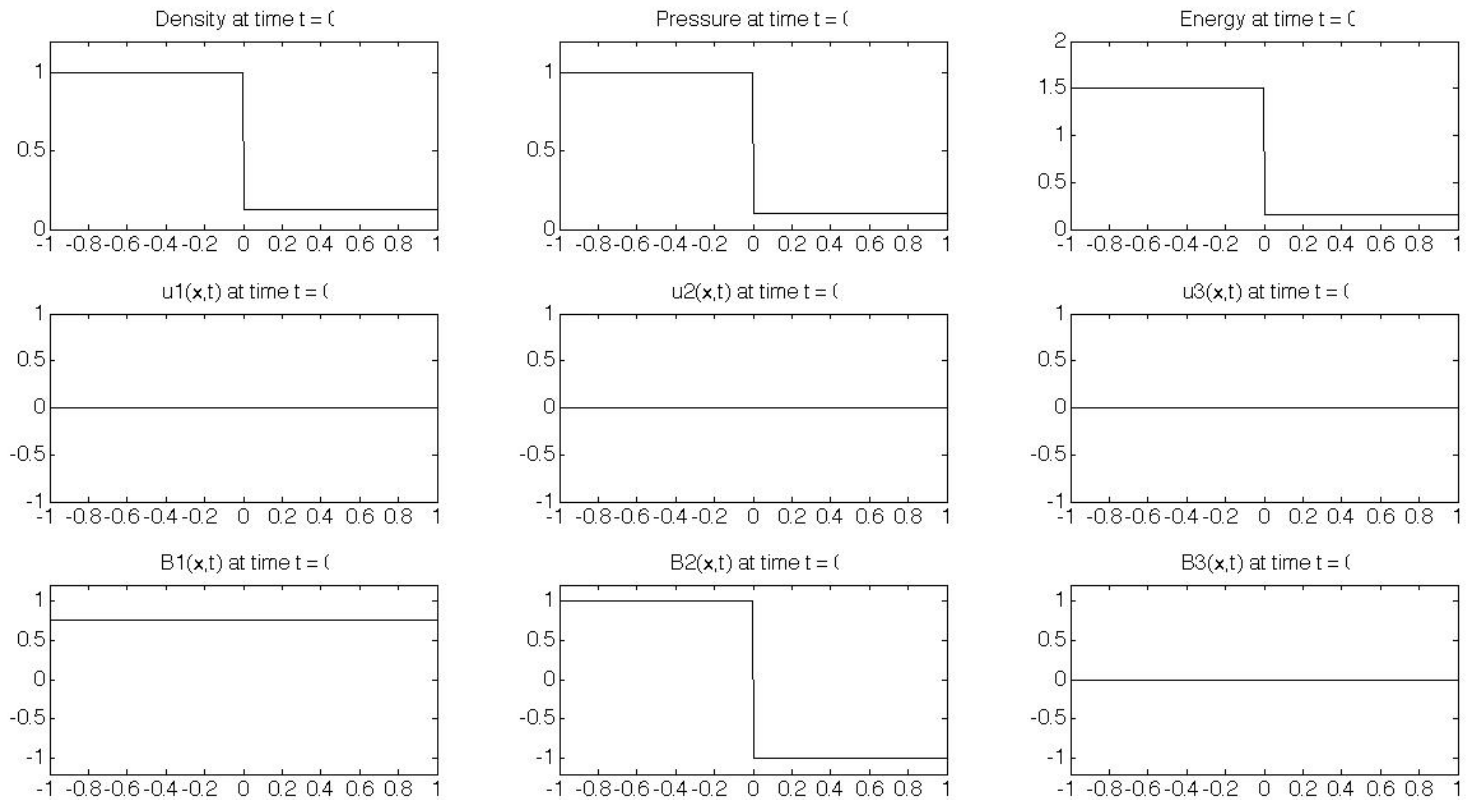
Close-up near MHD fast rarefaction wave.



Here at the peak in the MHD rarefaction wave region, the Yee scheme performs more poorly at coarse resolution, but better at fine resolution (compare the highly resolved peak in Fig. 3 of [?]).



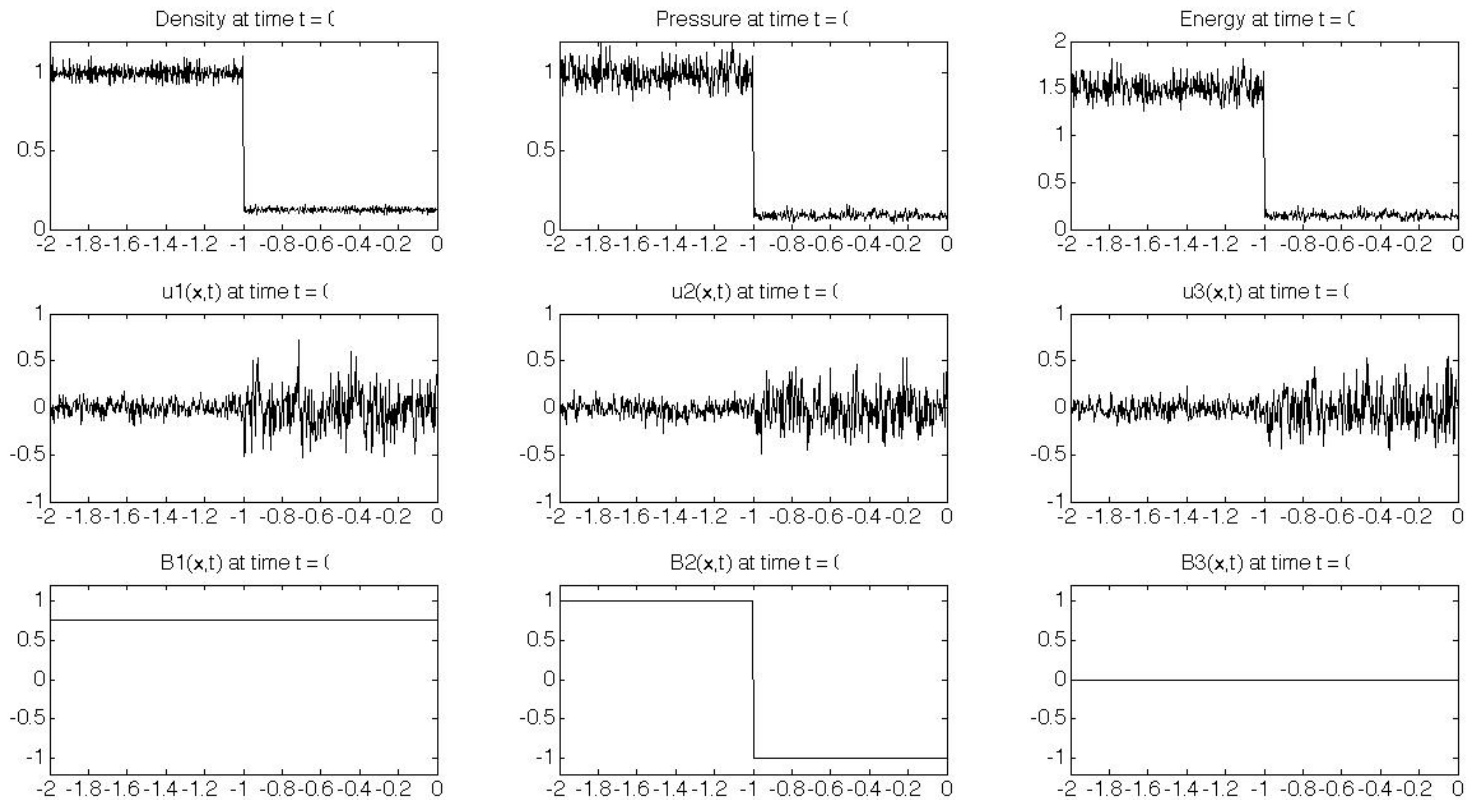
Computations: Brio-Wu ICs, ($t = 0$)



The initial conditions of the Brio-Wu problem.



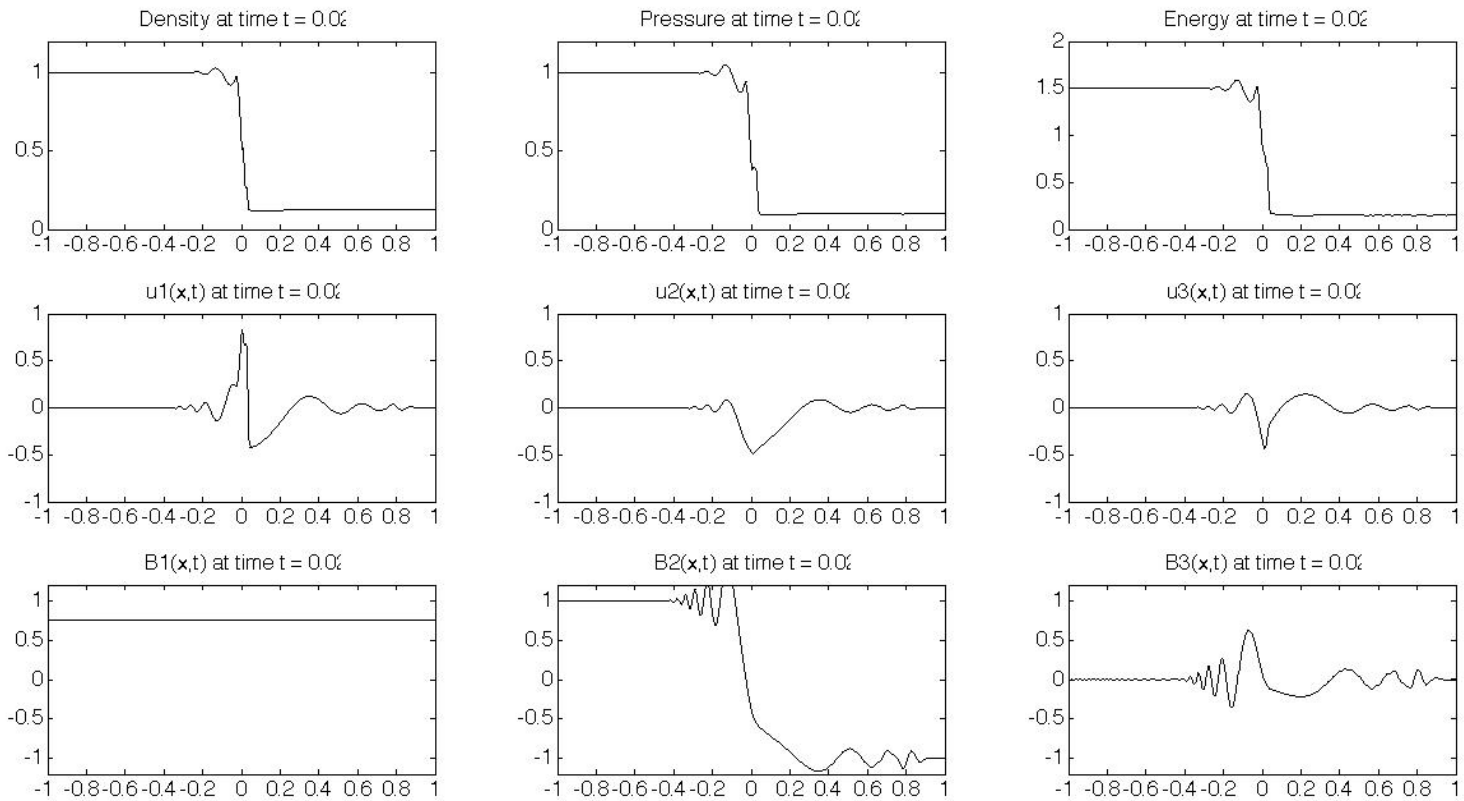
Computations: Brio-Wu kinetic ICs, ($t = 0$)



The initial conditions for a kinetic run of the Brio-Wu problem.



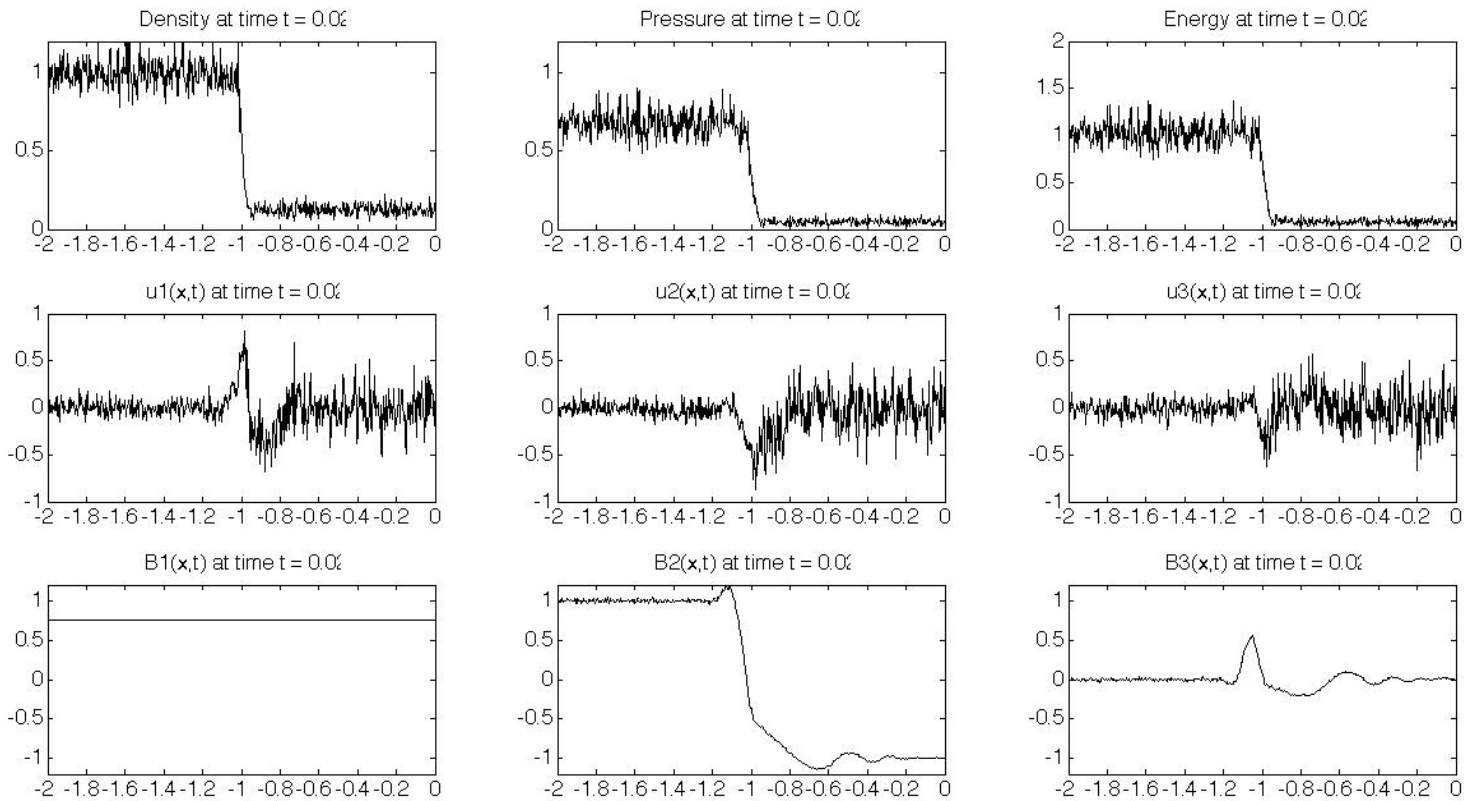
Computations: Brio-Wu 2-fluid, $r_L = 0.1, t = .02$ _____



Two-fluid Brio-Wu solution



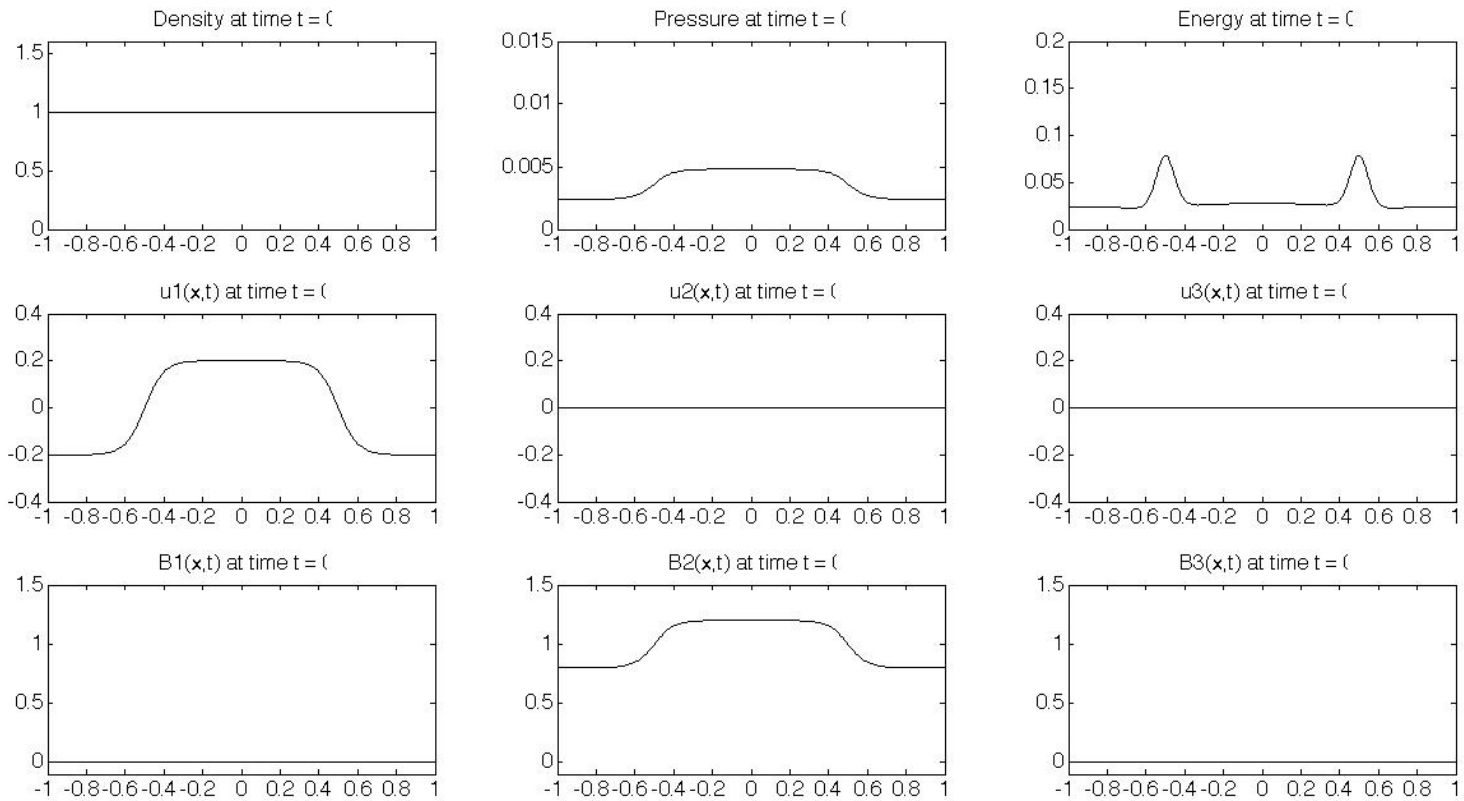
Computations: Brio-Wu kinetic, $r_L = 0.1, t = .02$ _____



Kinetic Brio-Wu solution



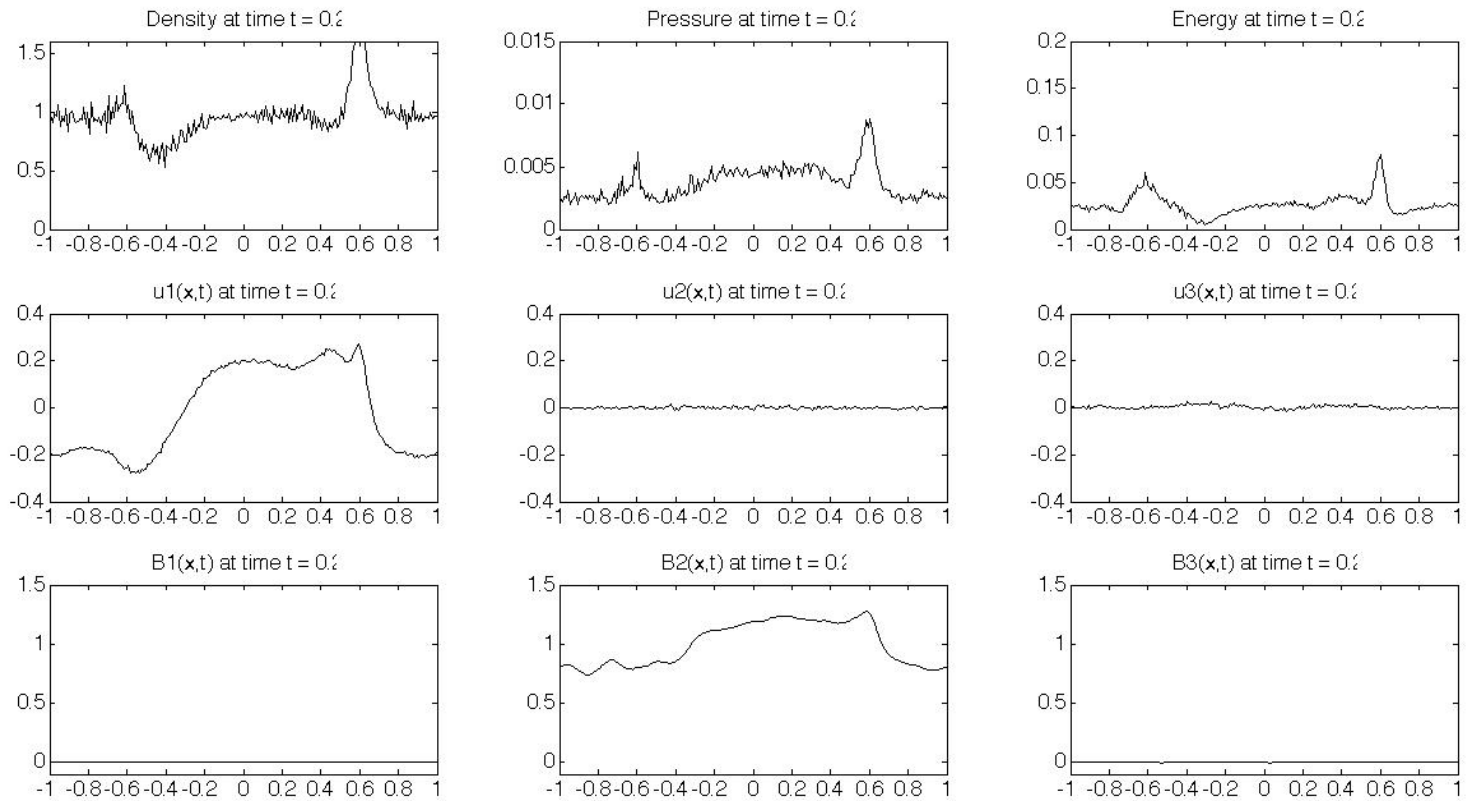
Computations: fast magnetosonic kinetic, $r_L = 0$ ---



Fast magnetosonic initial conditions



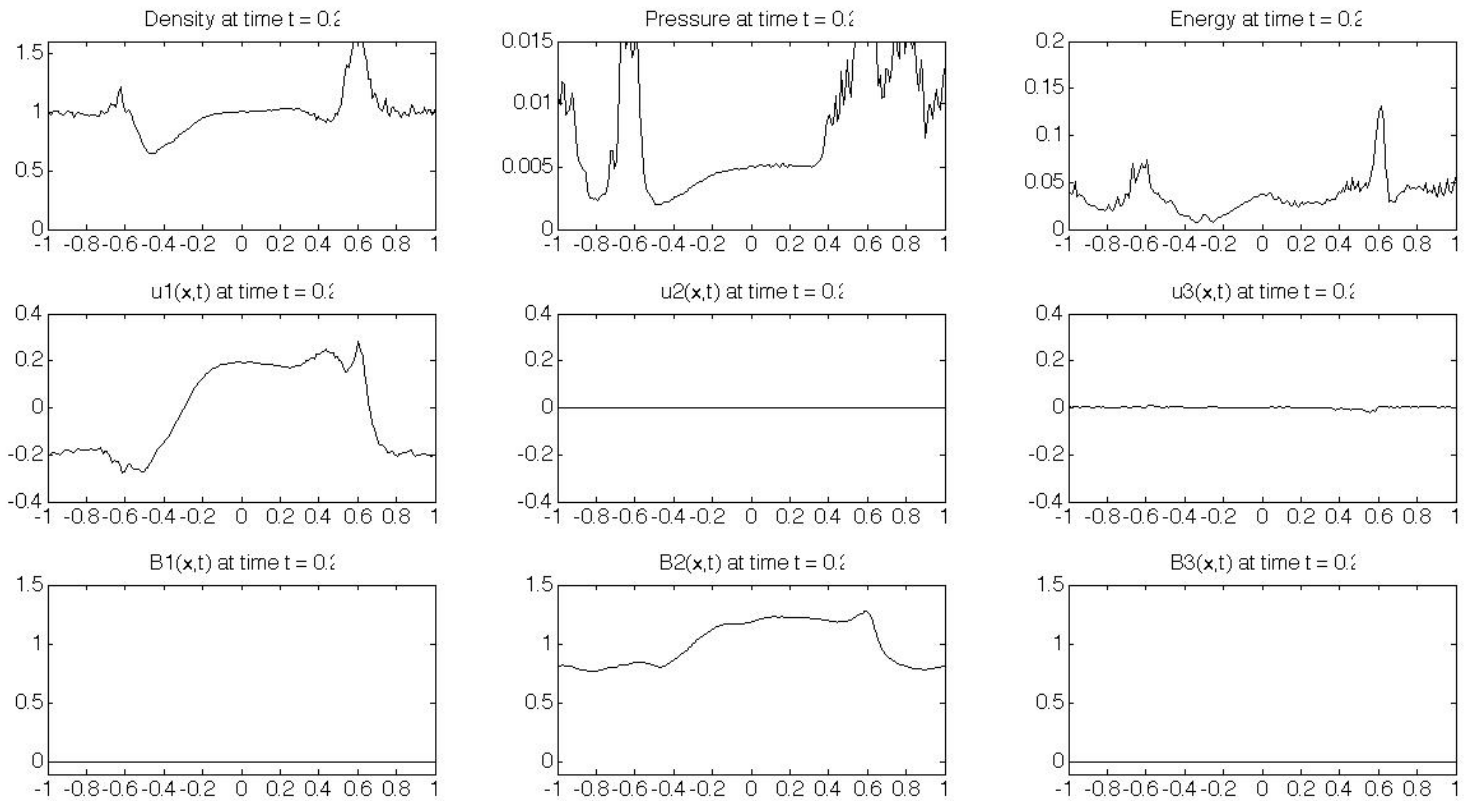
Computations: fast magnetosonic kinetic, $r_L = 0.2, t = .2$ _____



Kinetic fast magnetosonic solution



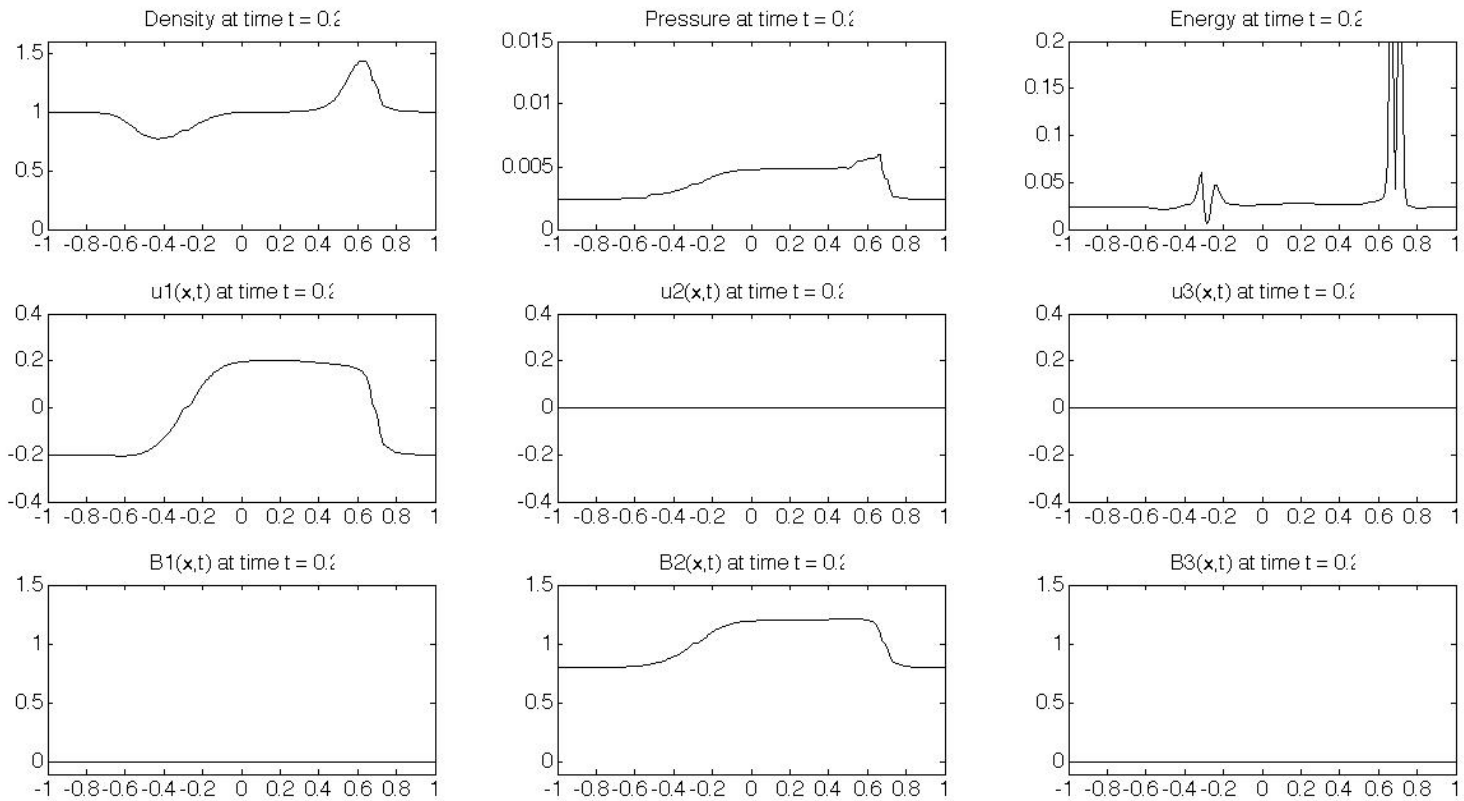
Computations: fast magnetosonic 2-fluid, $r_L = 0.2, t = .2$ _____



2-fluid fast magnetosonic solution



Computations: fast magnetosonic MHD, $r_L = 0.2, t = .2$ _____



MHD fast magnetosonic solution



Acknowledgements

- Wisconsin Space Grant Consortium
- My advisor, James Rossmanith
- Helpful conversations with Nick Murphy, James Drake, Ping Zhu, Andrew Christlieb, and Nick Hitchon.

